Characteristic Analysis of a Magnetically Actuated Capsule Microrobot in Medical Applications

Zhuocong Cai, Qiang Fu, Songyuan Zhang, Shuxiang Guo, *Fellow, IEEE*, Jian Guo, Xi Zhang, and Chunliu Fan

***Abstract*—A magnetic actuated capsule microrobotic system (MACMS) is proposed to control the microrobot to complete specific medical tasks, such as medical diagnosis or drug delivery. The structure design and control of the microrobot are optimized. By establishing the dynamic model of the microrobot with spiral structure, the optimal structure parameters are analyzed, and the fluid simulation of the propulsive force and the resistance of the microrobot are carried out by the finite element analysis software to obtain the optimal performance. During the experiment, the peristaltic pump was used for imitating the environment of the gastrointestinal tract, because the human intestinal tract is constantly peristaltic at random speeds. The experimental results indicated that by adjusting the rotational velocity and frequency of the rotating magnetic field, the magnetic actuated spiral jet microrobot could move flexibly in the pipeline where the fluid's peristaltic velocity is constantly changing medical functions at the desired area for diagnosis. The proposed microrobot and its optimization method make it possible for microrobot to be applied in medical practice.**

***Index Terms*—Magnetic actuated capsule microrobotic system (MACMS), spiral jet microrobot, finite element analysis, fixed-point inspection.**

I. Introduction

GASTRIC carcinoma has become a significant public health issues in the world. The prognosis of gastric carcinoma is closely related to the timing of diagnosis and treatment. The 5-year survival rate of patients with different stages of gastric cancer is significantly different. Early Gastric carcinoma can be cured by endoscopy, and the 5-year survival rate is more than 90% [1-3]. Wireless capsule endoscopy (WCE) has a great potential for human gastrointestinal (GI) examination and treatment in clinical medical applications; due to the advantages of safety, reliability, and painlessness [4-6], especially in the aspects of volume, driving mode, and medical practicability [7-9]. Imaging of Israel [3] proposed a wireless capsule endoscopy (M2A™ capsule endoscopy), which can move smoothly and painlessly in the human intestinal tract after swallowing. JINSHAN Group [10] developed a capsule endoscopy (OMOM capsule endoscopy), which has certain practicability in diagnosing intestinal diseases. Due to their movement rely on the intestinal peristalsis. In other words, because their movement is the passive moment and noncontrolled, the doctor cannot achieve repeat diagnoses in specific areas in clinical application [11].

Magnetically actuated microrobot has been widely studied to solve this problem [12-14]. Zhang et al. [15] proposed a variable-diameter capsule robot based on multiple wedge effects, actively using an external rotating magnetic field to move in the GI tract. Yim et al. [16] proposed a soft capsule endoscope, which controls the robot to roll to another position in the GI tract by the external magnetic field to achieve stable, continuous, and controllable movement. Kim et al. [17] proposed an oscillatory motion-based miniature magnetic walking robot, which makes the main body vibrate through the external magnetic field to generate thrust in the GI. Fu et al. [18] also proposed a magnetic actuated spiral jet microrobot, consisting of spiral jet and fin motion. Moreover, the structure parameters of the microrobot are discussed.

However, although some researchers have proved that the microrobot can move flexibly in the container filled with fluid, it is not enough to apply in the environment of human GI tract peristalsis at random speeds [13]. In order to solve the problem that the microrobot in the current research cannot maintain good mobility to perform medical functions under the environment of the random and continuous peristaltic speed of the human GI tract, this paper proposes a microrobot with a protective shell and its MACMS. The microrobot is controlled by its MACMS to maintain good mobility in the complex GI tract environment to achieve medical functions in areas requiring diagnosis.

This paper is organized as follows. Firstly, the MACMS for medical examination and treatment of the human GI tract is illustrated in Section 2. Secondly, the derivation of the dynamic model of the microrobot with spiral structure and the optimal parameters of the structure is developed in Section 3. In Section

This work was supported in part by Natural Science Foundation of Tianjin (18JCYBJC43200) and Tianjin Key Laboratory for Control Theory and Application in Complicated Systems (TJKL-CTACS-201903) and Innovative Cooperation Project of Tianjin Scientific and Technological Support (18PTZWHZ00090).

Corresponding authors: *Qiang Fu* and *Songyuan Zhang*.

Z. Cai, X. Zhang and C. Fan are with the Intelligent Robot Laboratory, Tianjin University of Technology, Tianjin 300380, China (e-mail: caizhuocong@hotmail.com; 549244209@qq.com; 2536723678@qq.com).

Q. Fu and J. Guo are with Tianjin Key Laboratory for Control Theory & Application in Complicated Systems and Tianjin International Joint Research and Development Center, Tianjin University of Technology, Tianjin 300380, China (e-mail: fuqiang6369@hotmail.com; gj15102231710@163.com).

S. Zhang is with State Key Laboratory of Robotics and System, Harbin Institute of Technology, Harbin 150001, China (e-mail: zhangsy@hit.edu.cn).

S. Guo is with the Department of Intelligent Mechanical Systems Engineering, Kagawa University, Takamatsu 761-0396, Japan (e-mail: guo@eng.kagawa-u.ac.jp).

4, the propulsive force and resistance of the microrobot are analyzed by using the finite element software, respectively. Section 5 describes that the magnetic actuated microrobot system's performance was evaluated using the peristaltic pump to simulate human intestinal peristalsis, and the experimental results were analyzed. Finally, conclusions and future work are illustrated. The measuring instrument of the magnetic actuated capsule microrobotic system proposed in this paper is used to measure the motion characteristics of the magnetically driven microrobot. The simulation method proposed measures and optimizes the structural parameters of the microrobot, and puts forward the measuring instrument and method of the propulsion and resistance of the microrobot, which can significantly improve the motion performance of the microrobot. Finally, a measurement method using a peristaltic pump to simulate human intestinal peristalsis is proposed, which can measure the motion characteristics of the microrobot in a fluid-filled environment, and the peristaltic speed is constantly changing, which further promotes the research of microrobot.

II. System Configuration

The conceptual design of MACMS is shown in Fig. 1(a). The doctor can accurately operate the capsule microrobot to complete medical tasks in the complex environment of the human intestinal tract through the remote control. The doctor can watch the images of the GI, providing real-time visual feedback. Furthermore, a positioning system consisted 6*6 magnetic sensor array is used to detect the posture and position of capsule microrobot by using the least square method. The magnetic actuated capsule microrobot system can significantly improve the success rate of examination and treatment. Less pain to the patient almost does not cause tissue trauma, thus reducing the time from hospitalization to rehabilitation [19-21].

A. Working Principle of Microrobot

Based on the previous research results [22], the magnetically actuated microrobot with spiral structure has been gained tremendous popularity in GI tract inspection, due to the advantage of spiral structure rotation, which transforms the radial rotation motion into the axis motion, the movement efficiency is relatively high in the narrow pipe. When the permanent magnet embedded in the microrobot rotates through the torque of the external magnetic field, the propeller pushes the fluid backward while generating a reaction force. Thus, the microrobot can move forward [23]. The model of microrobot is shown in Fig. 1(b).

Moreover, Fig. 1(c) shows how the microrobot rotates with an external magnetic field. When the magnetic dipole of the magnet tries to align with the local magnetic field, the magnetic dipole moment will be generated, so when the external magnetic field rotates inside, the permanent magnet inside the microrobot can rotate synchronously with the rotational frequency of the external magnetic field [19, 22]. Therefore, the working process of robots in the human body is summarized as follows:

Step 1: The patient swallows microrobots and they reach the stomach of the initial position. Then, the reaction force of the fluid is used to make the microrobots gain propulsion and move. Then, the external magnetic field is used to control the rotation of the spiral propulsion mechanism inside of microrobots. For instance, when the magnetic field is controlled by clockwise rotation in the X-Z plane, microrobots move forward in the Y direction if it is necessary to move backward by controlling the magnetic field to rotate anticlockwise in the X-Z plane.

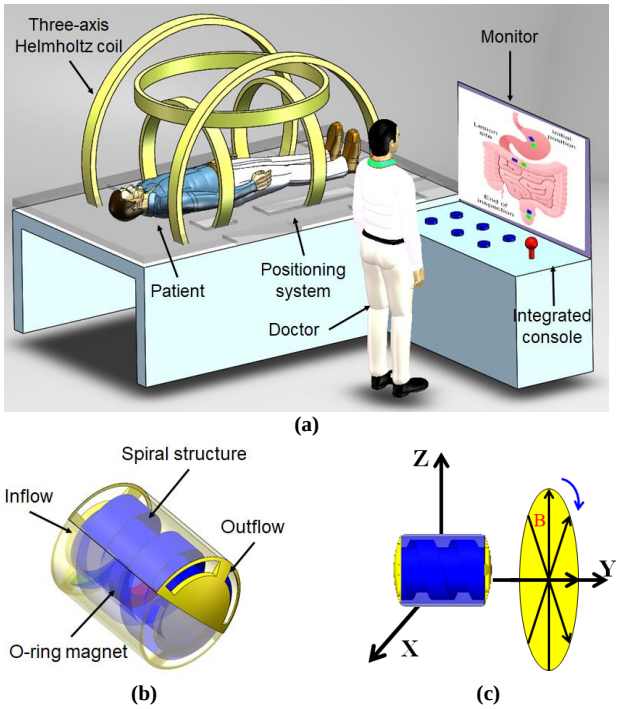

Fig. 1. (a) Overall of the control system and principle of medical tasks by using the magnetic actuated microrobot. (b) Model of the spiral jet microrobot. (c) Motion principle of the microrobot.

TABLE I
THREE-AXIS HELMHOLTZ COIL PARAMETERS

	X axis	Y axis	Z axis
Coil radius(mm)	293.4	211.4	157.4
Coil length(mm)	293.4	211.4	157.4
Number of turns	216	174	126
Resistance(Ω)	5.52	3.29	1.86
Material	Cu	Cu	Cu

Step 2: When the microrobots move to the lesion site and need to perform medical functions, the external magnetic field controls the microrobot of the image module to move to the lesion location, providing a safe guarantee for doctors to operate the microrobot of the functional module. Then doctors can control another microrobot to perform tasks, such as targeted medical treatments.

Step 3: After tasks are completed, microrobots are discharged from the patient's body together. Through the cooperative control of microrobots, they can pass through the narrow or curved part of the human intestinal tract.

According to the above steps, doctors can control microrobots to diagnose and treat any parts of the human GI tract by adjusting the direction and parameters of the external magnetic field on any plane, obtaining the position of the microrobots through the magnetic tracking approach [24, 25], to realize the

medical function of the microrobots. In this process, the optimal number of microrobots is two: one microrobot with a functional module acts as the doctor's hand to perform medical functions, and the other microrobot with image module acts as the doctor's eye to guarantee examination and treatment. However, the limitations of the clinical application of microrobots are also noteworthy. The biggest challenge is the high cost of microrobots, so the price cannot meet most consumers who need gastrointestinal examination and treatment. Meanwhile, because the external magnetic field controls microrobots, people with metal implants, such as heart stents, cannot be examined and treated with magnetically driven microrobots.

B. *External Rotational Magnetic Field*

In order to precisely control the rotation direction and speed of the permanent magnet embedded in the microrobot's spiral structure, the three-axis Helmholtz coil is used as the role of providing energy, and the rotation speed of the microrobot is controlled by controlling the frequency of the magnetic field [22]. The parameter of each axis has shown in Table I.

According to Biot-Savart law, the magnetic flux density of any point on the axis of each pair of Helmholtz coils can be calculated by:

$$B=\frac{i\mu NR^2}{2}\left[\left\{R^2+\left(\frac{L}{2}-x\right)^2\right\}^{-\frac{3}{2}}+\left\{R^2+\left(\frac{L}{2}+x\right)^2\right\}^{-\frac{3}{2}}\right] \quad (1)$$

Where B is the magnetic flux density, i is the current flowing into the coil, μ is the vacuum permeability, L is the distance between a pair of coils, and x is an arbitrary position from the center of a pair of coils.

Furthermore, the magnetic force **F** and the magnetic torque **T** are defined by [7]:

$$\mathbf{T}=\mu_0 V\mathbf{M}\times\mathbf{H} \quad (2)$$

$$\mathbf{F}=\mu_0 V(\mathbf{M}\cdot\nabla)\mathbf{H} \quad (3)$$

Where μ_0 is the permeability of free space, V is the volume of the magnet, **M** is the magnet's magnetization, and ∇ represents a gradient operator.

In the three axes of X, Y and Z, each axis has a pair of coils. The radius of each pair of coils is R, equal to the distance L between the corresponding coils. When each pair of coils receives the same current, according to the law, the flux density generated is shown as [26]:

$$\mathbf{B}=\begin{bmatrix}B_x\\B_y\\B_z\end{bmatrix}=\begin{bmatrix}B_0\sin\alpha\sin(\omega t-\varphi_x)\\-B_0\sin\beta\sin(\omega t-\varphi_y)\\B_0\sin\gamma\sin(\omega t+\pi/2)\end{bmatrix} \quad (4)$$

Where B_x, B_y, and B_z denote the magnetic flux densities of the X-axis, Y-axis, and Z-axis, respectively; α, β, and γ denote the angles between the moving direction of the microrobot and the X-axis, Y-axis, and Z-axis; $\tan\varphi_x=(\cos\alpha\cdot\cos\gamma/\cos\beta)$, $\tan\varphi y=(\cos\beta\cdot\cos\gamma/\cos\alpha)$.

According to the characteristics of the three-axis Helmholtz coil, the same coil model as the actual experimental platform is established by the industrial electromagnetics simulation software. The model is carried out in Fig. 2(a) [26].

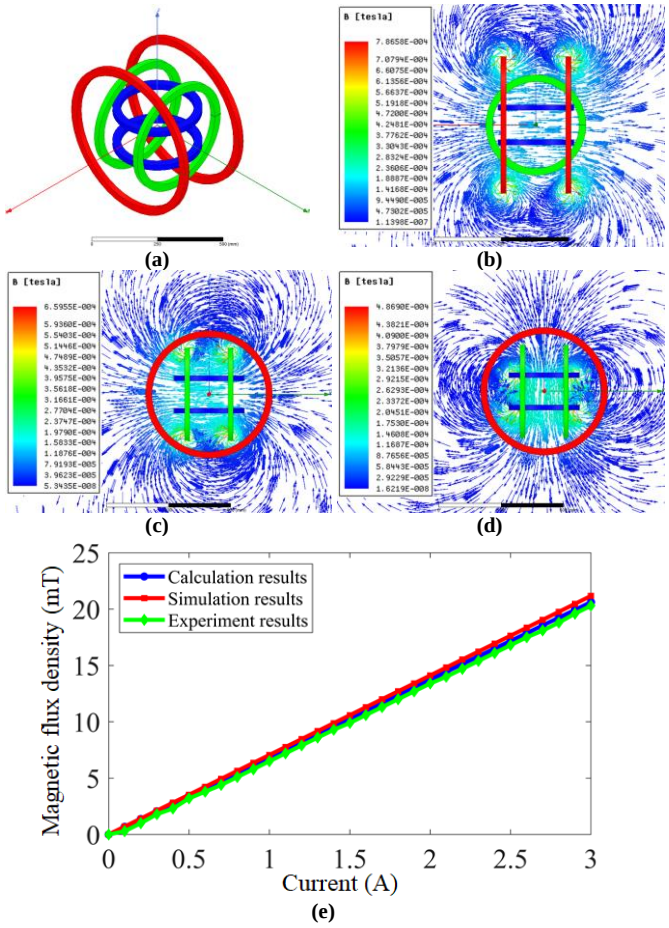

Fig. 2. (a) Model of the three-axis Helmholtz coil. (b) Magnetic flux density of X-coil. (c) Magnetic flux density of Y-coil. (d) Magnetic flux density of Z-coil. (e) Relationship between the current and magnetic flux density.

By applying the same current to each pair of coils, the results of the magnetic flux density of the cross-section in the three-axis directions are shown in Fig. 2 (b), (c), and (d). It can be observed that a specific range of uniform magnetic fields is generated in the central region applying the same current (1A) to each pair of coils. Through measurement by using a Gauss meter (CH-Hall Model 1600 Gauss/Tesla meter), the uniform area obtained is consistent with the ideal uniform area of the experimental device, which is 200*200*100mm. The linear relationship between magnetic induction and current is shown in Fig. 2(e). It can be concluded that the effective rate of the actual magnetic induction intensity is 99.35%, indicating that the microrobot can maintain a highly controllable state in the uniform area of the experiment.

III. Modeling

According to the hydrodynamic theory, a model is built to analyze the characteristic of the microrobot in pipe [27], as shown in Fig. 3.

The Reynolds numbers in a pipe are generally defined as:

$$\mathrm{Re}=\frac{\rho U d}{\mu} \quad (5)$$

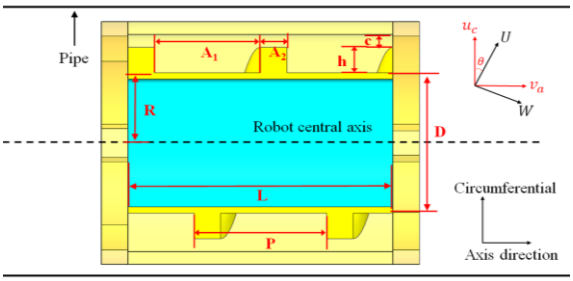

Fig. 3. Dynamic model of microrobot.

Where ρ is the density of the fluid. U is the velocity of the microrobot, d is the pipe's hydraulic diameter and μ is the coefficient of kinematic viscosity.

For the convenience of analysis, the coordinate axis is built-in Fig. 3, u_c and v_a are defined as circumferential and axis velocity respectively. U and W are the velocity projections of u_c and v_a along and perpendicular to the helical direction. Moreover, θ is the angle of the microrobot spiral. In order to simplify the calculation, two dimensionless parameters are presented, $A_1 = (1\text{-}\beta)\ a$, $A_2 = \beta a$, $h = \gamma c$. Then U and W can be combined by u_c and v_a:

$$W = v_a \cos\theta - u_c \sin\theta \tag{6}$$

$$U = u_c \cos\theta + v_a \sin\theta \tag{7}$$

According to the Reynolds number equation, $p_1(x)$ and $p_2(x)$ are the pressure distributions in the areas of A_1 and A_2 respectively, which are obtained as follows:

$$p_1(x) = \frac{6\mu\gamma(1-\beta)W_1^2 x}{c^2(1+\gamma)^2\left[(1-\beta)W_1 + \beta(1+\gamma)^3 W_2\right]} \tag{8}$$

$$p_2(x) = -\frac{\left(6\mu\beta\gamma(1+\gamma)^2 W_2^2\right)(a-x)}{c^2\left[(1-\beta)W_1 + \beta(1+\gamma)^3 W_2\right]} \tag{9}$$

Furthermore, according to Navier-Stokes equations, the force balance of fluid elements on the surface of the spiral structure is analyzed:

$$\left.\begin{aligned} \frac{\partial P}{\partial x} &= \mu\frac{\partial^2 U_x}{\partial z^2} \\ \frac{\partial P}{\partial y} &= \mu\frac{\partial^2 U_y}{\partial z^2} \\ \frac{\partial P}{\partial z} &= \mu\frac{\partial^2 U_z}{\partial z^2} \end{aligned}\right\} \tag{10}$$

Where P is the dynamic pressure of the fluid between the spiral surface and the pipe wall.

According to the theory of hydrodynamic lubrication and Newton's law of internal friction, the shear stress of the microrobot under the action of fluid can be expressed as:

$$F_x = \iint\left(-\frac{h}{2}\frac{\partial p}{\partial x} - \frac{\mu W}{h}\right)dydx \tag{11}$$

$$F_y = \iint\left(-\frac{h}{2}\frac{\partial p}{\partial y} - \frac{\mu U}{h}\right)dydx \tag{12}$$

Where F_x is the shear stress of the microrobot under the action of the fluid on the X-axis, F_y is the shear stress of the microrobot under the action of the fluid on the Y-axis.

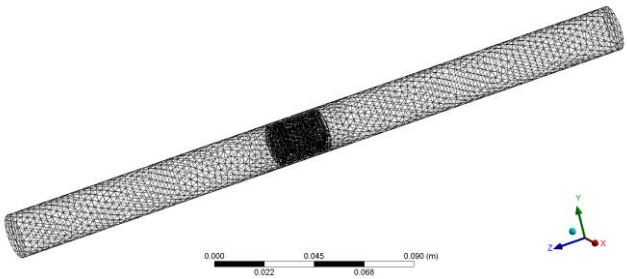

Fig. 4. Simulation grids of the model of the microrobot.

TABLE II
SPECIFICATIONS OF THE MICROROBOT

Type	Parameters
Length of microrobot(mm)	24
Radial of microrobot(mm)	9
Length of thread(mm)	20
Diameter of thread (mm)	11
Height of thread(mm)	2
Width of thread(mm)	2
Pitch of thread(mm)	20
Thickness of shell(mm)	1

Therefore, when the spiral structure of the microrobot rotates, the propulsive force is expressed as:

$$F_{pro} = F_y \sin\theta - F_x \cos\theta \tag{13}$$

$$F_{res} = F_y \cos\theta + F_x \sin\theta \tag{14}$$

In order to obtain the optimal structure parameter of the microrobot in the human GI tract, the optimum solution is obtained using FDM (Finite Difference Method). Where F_{pro} is the propulsive force of the microrobot in motion, F_{res} is the resistance of the microrobot in motion. Studies indicated that when the γ is 3, β is 0.53 and θ is 45°, the microrobot can obtain the optimal velocity [28]. The operator can select the best structural parameters of the microrobot according to specific needs.

IV. Dynamic Analysis of the Microrobot

A. Establishment of Simulation Model

The method of controlling a single variable has been used to evaluate the optimal motion state of the model in this dynamic simulation due to the number of variables being large and complex when the microrobot moves in the pipeline full of fluid. As a result of the main factors affecting the propulsive force and the resistance are different, which is divided into two parts to study. Therefore, the Computational Fluid Dynamics (CFD) analysis is carried out using the screw jet microrobot whose structural parameters are shown in Table II, and the relationships between the rotational speed and the propulsion force, the axial speed and the resistance are introduced respectively.

Fig. 4 shows the dynamic grid division of the model of the microrobot, which is divided into two parts: the microrobot model and the pipeline model. The mesh size of the static flow field of the pipe model is slightly larger, the mesh size of the

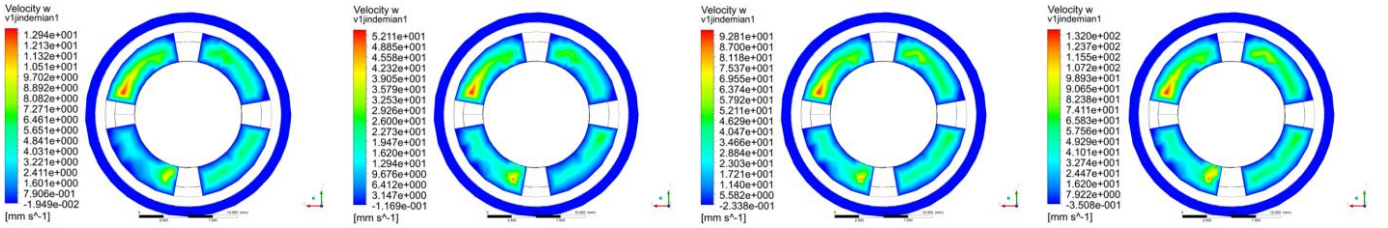

(a) ω=20rad/s **(b)** ω=120rad/s **(c)** ω=240rad/s **(d)** ω=360rad/s

Fig. 5. Simulation results on inlet plane velocity contour with different rotational speed of the microrobot.

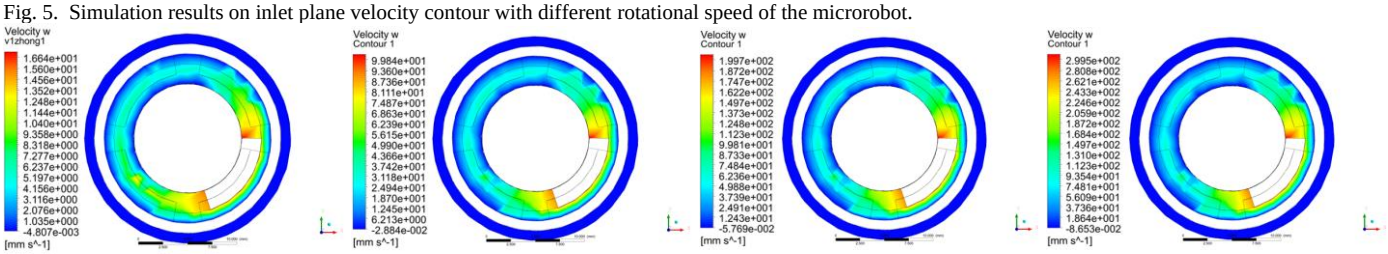

(a) ω=20rad/s **(b)** ω=120rad/s **(c)** ω=240rad/s **(d)** ω=360rad/s

Fig. 6. Simulation results on middle plane velocity contour with different rotational speed of the microrobot.

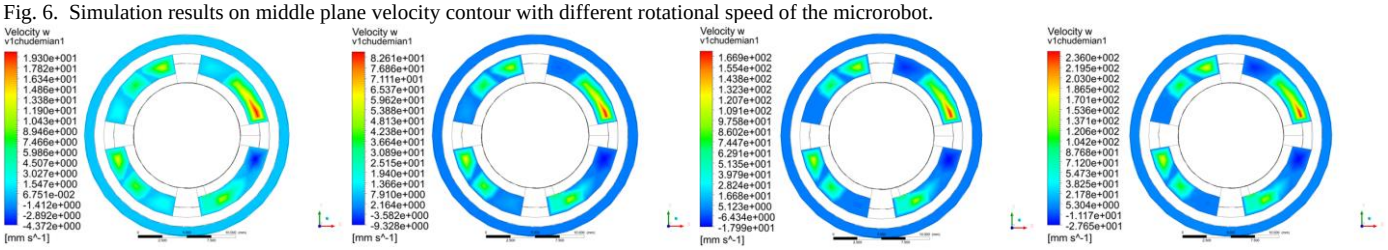

(a) ω=20rad/s **(b)** ω=120rad/s **(c)** ω=240rad/s **(d)** ω=360rad/s

Fig. 7 . Simulation results on outlet plane velocity contour with different rotational speed of the microrobot.

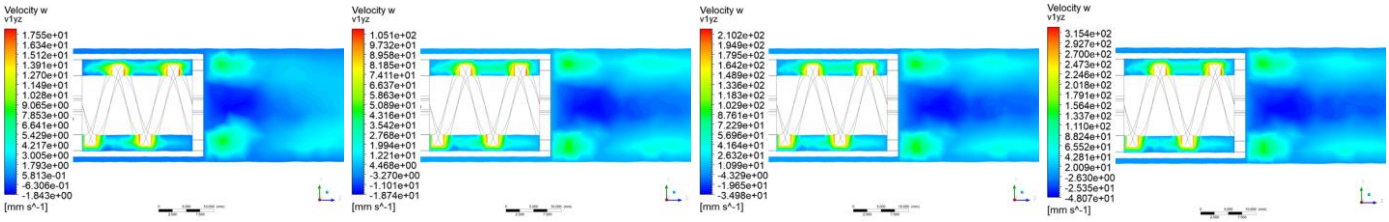

(a) ω=20rad/s **(b)** ω=120rad/s **(c)** ω=240rad/s **(d)** ω=360rad/s

Fig. 8. Simulation results on axis-plane velocity contour with different rotational speed of the microrobot.

dynamic flow field of microrobot with improved overall mesh quality model is relatively small; in order to balance the accuracy and efficiency of simulation when the microrobot moves in the pipeline [29]. Since the shape of the intestine is similar to a cylinder, the regular three-dimensional cylinder is used in the calculation area to simulate the intestine, and the fluid is set to flow in the positive direction along the z-axis. In order to prevent the accuracy of the calculation results from being affected when the microrobot approaches the inlet or outlet of the pipe, the microrobot model is placed in the middle of the pipe, and the whole length of the pipe is equal to the unit length of seven microrobots [30].

In order to establish an axial hydrodynamic model, there are several assumptions [31]. First of all, the intestinal deformation is not considered, and the microrobot's centre axis coincides with the pipeline's centre axis. Secondly, water is used as the experimental fluid of this simulation, which is regarded as a viscous incompressible fluid. Finally, since the primary purpose of this study is to investigate the force of horizontal movement of the microrobot, the force in the vertical direction of the microrobot, such as gravity and buoyancy, is ignored, and only by propulsive force and resistance to affect the movement of the microrobot.

The microrobot is rotating and moving in the intestinal tract full of mucus in the actual medical examination. Undoubtedly, the simulation calculation in the intestinal tract needs to be able to solve the complex external flow, rotating flow field and other problems. By understanding the Reynolds number criterion, in order to get more accurate results in the numerical calculation, the solution method is set as the turbulence model k-epsilon model, which is widely applicable, reliable and convergent, and especially suitable for the external flow problems of complex geometry like the intestinal tract in this simulation, namely k-ε model [29]. In the k-ε model, the Realizable model, most suitable for the actual situation of rotating flow calculation, is applied to simulate. The Semi-Implicit Method for Pressure-Linked Equations (SIMPLE) algorithm solves the coupling equations of pressure and velocity in the simulation, because the fluid is incompressible.

B. Propulsive Force Analysis of the Microrobot

Since this section only analyzes the microrobot's motion state in the container full of fluid from the dynamic point of view, it does not consider the speed that the robot cannot reach

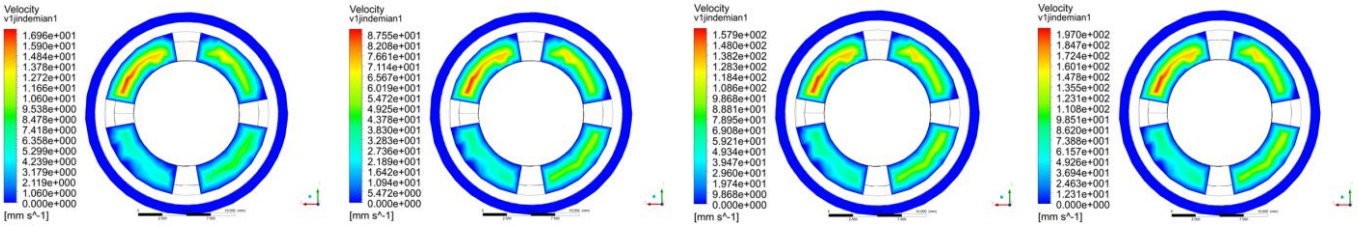

(a) *v*=5mm/s **(b)** *v*=35mm/s **(c)** *v*=70mm/s **(d)** *v*=100mm/s

Fig. 9. Simulation results on inlet plane velocity contour with different axial velocity of the microrobot.

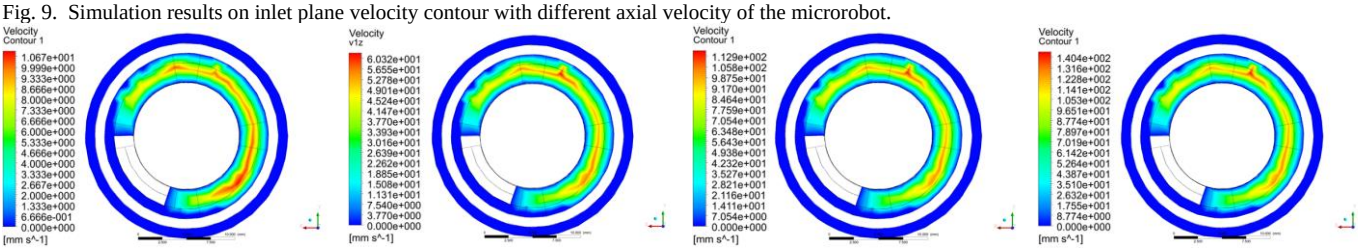

(a) *v*=5mm/s **(b)** *v*=35mm/s **(c)** *v*=70mm/s **(d)** *v*=100mm/s

Fig. 10. Simulation results on middle plane velocity contour with different axial velocity of the microrobot.

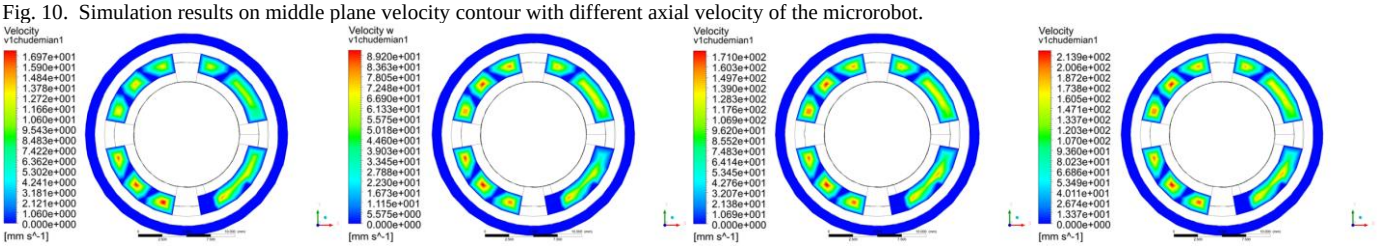

(a) *v*=5mm/s **(b)** *v*=35mm/s **(c)** *v*=70mm/s **(d)** *v*=100mm/s

Fig. 11. Simulation results on outlet plane velocity contour with different axial velocity of the microrobot.

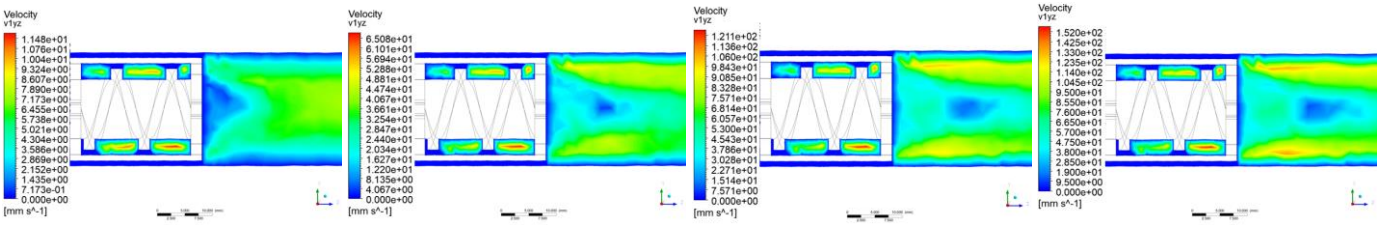

(a) *v*=5mm/s **(b)** *v*=35mm/s **(c)** *v*=70mm/s **(d)** *v*=100mm/s

Fig. 12. Simulation results on axis-plane velocity contour with different axial velocity of the microrobot.

in the actual situation. By finite element analysis software, a dynamic modal based on geometrical parameters is established with a rotating speed of 0 rad/s to 360 rad/s and an increment of 20 rad/s to evaluate the effect of rotating speed on the propulsive force. Moreover, in the whole propulsive force fluid simulation, the inlet and outlet of the pipe are set as the standard atmospheric pressure outlet. Because the overall position of the microrobot in the pipe is unchanged, the microrobot will not be subject to resistance during the rotation of the spiral structure.

The velocity contour of the fluid flowing into the microrobot inlet surface is shown in Fig. 5. It shows that the fluid velocity at the entrance increases with the increase of the rotation speed of the microrobot. When the spiral structure rotates at high speed, the fluid velocity attached to it is much faster than other parts, so it is red on the velocity contour.

The velocity contour of the middle plane surface of the fluid outflow microrobot is shown in Fig. 6. The results show that the fluid velocity in the middle part of the microrobot increases with the microrobot rotation speed. However, the fluid velocity outside the microrobot hardly changes, proving the microrobot shell's reliability for human intestinal protection.

The velocity contour of the outlet surface of the fluid outflow microrobot is shown in Fig. 7. It is shown that the fluid velocity at the outlet increases with the rotation speed of the microrobot. The velocity at the outlet is much faster than that at the inlet at the same speed due to the rotation of the screw structure.

The axial plane velocity contour of the fluid in the pipeline is shown in Fig. 8. It shows that the fluid velocity increases with the rotational speed. When the rotational speed of the spiral structure is too low, the liquid at the tail of the microrobot may not spray evenly, which may lead to random shaking of the robot and damage to the intestinal tract.

C. Resistance Analysis of the Microrobot

For resistance analysis, the axial velocity of the robot is a crucial factor. However, the finite element simulation software is more convenient to set fluid motion and boundary parameters, and the data is more accurate when analyzing the whole moving object. Therefore, setting the fluid velocity as the motion velocity of the microrobot can better analyze the influence of resistance on the microrobot. On this basis, the fluid velocity is set as 0 mm/s to 100 mm/s, the increment of 5 mm/s is used as the velocity of the microrobot, and the pipeline entrance surface is set as the velocity entrance surface, the whole microrobot moves axially at a certain velocity.

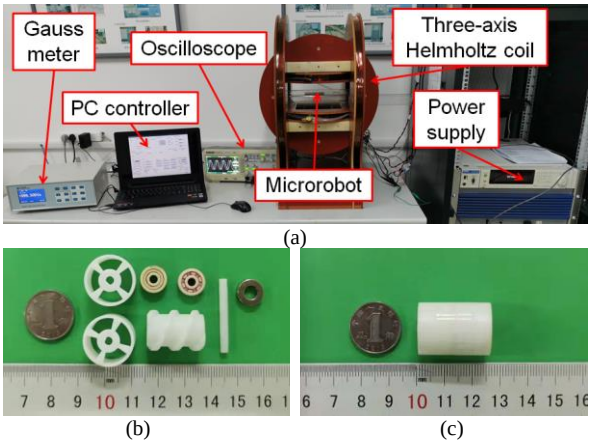

Fig. 13. (a) The Electromagnetic Actuation System. (b) The structure of microrobot. (c) The prototype of microrobot.

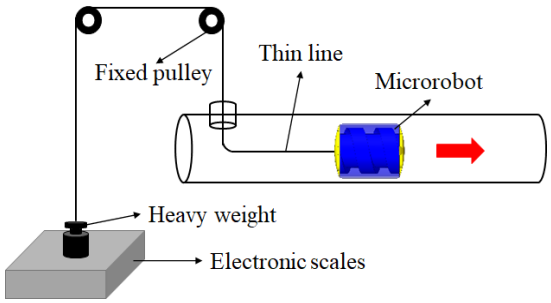

Fig. 14. Measurement system of the motion performance of the microrobot.

The velocity contour of the fluid flowing into the microrobot inlet surface is shown in Fig. 9. The results show that the velocity of the inlet fluid increases with the increase of the axis velocity of the microrobot. Due to the viscous force, the velocity of the fluid in contact with the spiral structure is low, so the velocity contour is blue.

The velocity contour of the middle plane surface of the fluid outflow microrobot is shown in Fig. 10. The results show that with the increase of the axial velocity of the microrobot, the fluid velocity in the middle of the microrobot increases. In contrast, the fluid velocity outside the microrobot changes little, proving the microrobot shell's reliability for human intestinal protection.

The velocity contour of the outlet surface of the fluid outflow microrobot is shown in Fig. 11. The results show that the fluid velocity at the outlet increases with the increase of the axial velocity of the microrobot.

The axial plane velocity contour of the fluid in the pipeline is shown in Fig. 12. The results show that the fluid velocity increases with the increase of the axial velocity of the microrobot. Moreover, the flow direction of the fluid flowing out of the microrobot outlet is uniform with the increase of the axial velocity of the microrobot.

V. Experiment Results

The MACMS was used to test the motion performance of the magnetic actuated spiral jet microrobot with a protective shell, as shown in Fig. 13(a). The microrobot is placed in a uniform rotating magnetic field region generated by a three-axis Helmholtz coil. When the PC controller sends signals to the

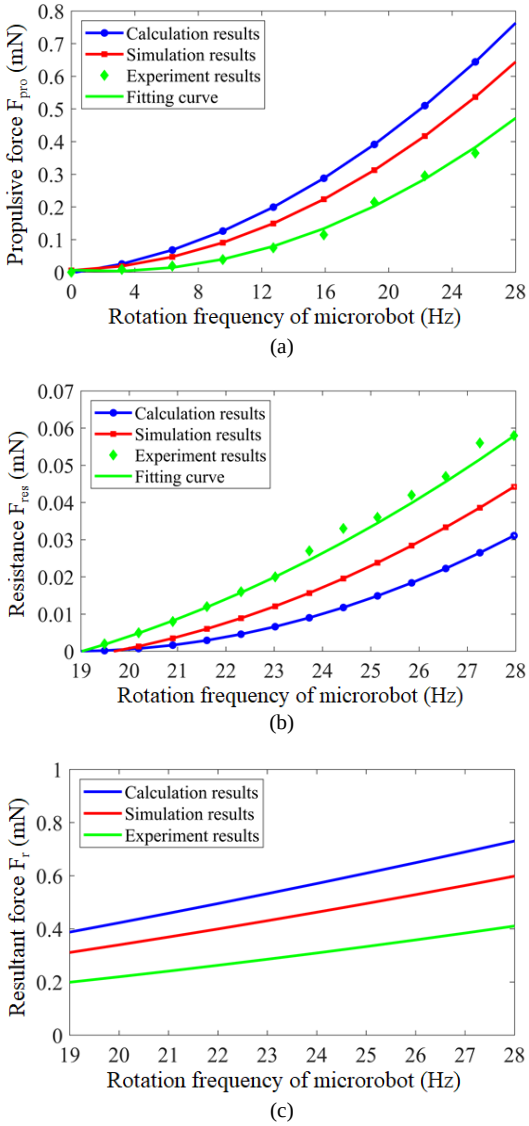

Fig. 15. (a) Relationship between propulsive force and rotation frequency of the microrobot. (b) Relationship between resistance and rotation frequency of the microrobot. (c) Relationship between resultant force and rotation frequency of the microrobot.

MACMS, the coil of the slave will generate a rotating magnetic field to provide energy for the microrobot. By adjusting the magnetic field frequency from 0 Hz to 50 Hz, the direction of the rotating magnetic field is adjusted to control the rotation velocity and motion direction of the microrobot in the fluid-filled pipe [32]. The measurement system of propulsion force and resistance of microrobot consists of thin lines, a heavy weight, and electronic scales, as shown in Fig. 14. Our team prior to imaging features of the microrobot research, image acquisition module encapsulation well into the microrobot, PC controller to connect to wireless receiving module, image in the process of microrobot movement, the appearance of the target is clear, the entire imaging process time is 20 s, indicating that the microrobot can realize the function of real-time image information collection [33]. Fig. 13(b) shows the structure of the microrobot 3D printed by medical resin, Fig. 13(c) shows the prototype of the microrobot, and the size is consistent with table II.

A. *Motion performance of the microrobot*

The relationship between the propulsive force and rotation frequency of the microrobot and the relationship between the resistance and rotation frequency of the microrobot are shown in Fig. 15(a) and Fig. 15(b). The results show that the propulsive force and resistance of the microrobot increase exponentially with the increase of rotational frequency. However, due to the influence of friction in the experiment, the experimental propulsion force is less than the calculation and simulation results. Although the rotation of the spiral structure of the microrobot generates propulsion force, the microrobot cannot move because it cannot overcome the maximum static friction force. Until the rotation frequency reaches 19 Hz, the microrobot can move and produce resistance. When the rotation frequency raised to 28 Hz, the microrobot's internal permanent magnet cannot keep the same rotation frequency with the magnetic field and enters the cut-off state, so the microrobot's resistance measurement range is 19 Hz to 28 Hz. Due to friction's influence, the experiment's resistance measured is higher than the calculation and simulation results. The resultant force F_r of the microrobot in motion is expressed as:

$$F_r = F_{pro} - F_{res} \tag{15}$$

Where F_{pro} is the propulsive force of the microrobot, F_{res} is the resistance of the microrobot. Fig. 15(c) shows the results of the resultant force of the microrobot when the microrobot is moving. The curvatures of the curves of calculation, simulation and experiment are k_1, k_2 and k_3 respectively, which can be obtained:

$$\begin{cases} k_1 = \dfrac{7.6\times10^{-4}}{\left(1.007+7.6\times10^{-4} f\right)^{\frac{3}{2}}} \\ k_2 = \dfrac{8.11\times10^{-4}}{\left(1.01+8.11\times10^{-4} f\right)^{\frac{3}{2}}} \\ k_3 = \dfrac{7.48\times10^{-4}}{\left(1.006+8.11\times10^{-4} f\right)^{\frac{3}{2}}} \end{cases} \tag{16}$$

Where f is the rotation frequency of the microrobot in motion. The difference between the curvatures of the curves of the three results is less than 0.1%, indicating that the three curves have a very close bending degree, which proves that the growth degree of the resultant microrobot force of the three results is the same. However, because the friction cannot be eliminated in the experiment, and there are errors in the geometric dimensions of the microrobot, and the pipeline, the resultant force of the microrobot in the experimental results is less than that in the calculation and simulation results.

B. *Flexibility of microrobots in clinical applications*

During the experiment, the changing frequency of the magnetic field was adjusted at 1 Hz per order in a transparent tube with a diameter of 26 mm. The peristaltic pump was used to simulate the peristaltic environment of the human intestinal tract because of the persistent peristalsis of the human intestinal

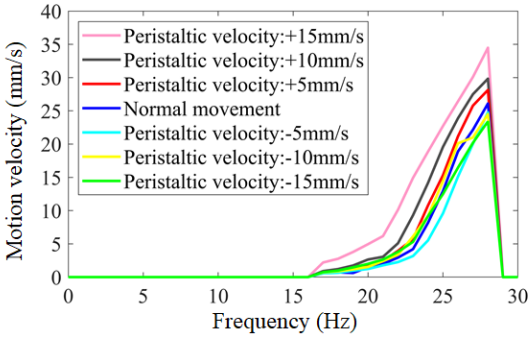

Fig. 16. Relationship between motion velocity of the microrobot and frequency.

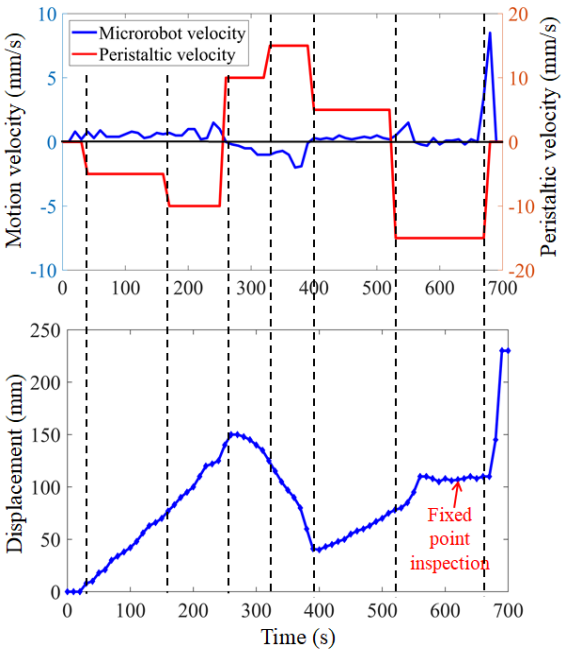

Fig. 17. Process of microrobot performing medical inspection task.

tract. The relationship between the velocity of the microrobot and the rotation frequency of the magnetic field was measured under the condition that the stagnant water and the peristaltic speed of the peristaltic pump were +15 mm/s, +10 mm/s, 5 mm/s, -15 mm/s, -10 mm/s, -5 mm/s respectively. The maximum speed of the microrobot is 26.78 mm/s in the still water, 34.81 mm/s in the peristaltic speed of peristaltic pump +15 mm/s, and 23.01 mm/s in the peristaltic speed of peristaltic pump -15 mm/s. The experimental results show a linear relationship between the magnetic field frequency and the moving velocity between 17 Hz and 28 Hz, as shown in Fig. 16, and the microrobot's forward and backward motion performance is the same. It is because when the magnetic field frequency is lower than 17 Hz, the magnetic torque generated by the magnetic field cannot overcome the maximum static torque of the microrobot itself. This phenomenon is defined as the starting frequency of the microrobot. When the magnetic field frequency exceeds 28 Hz, the phenomenon that the internal permanent magnet of the microrobot cannot synchronize with the rotating magnetic field; cannot produce enough propulsive force to overcome the fluid's resistance is defined as the cut-off frequency of the microrobot. In other words, in medical applications, to make the microrobot can be

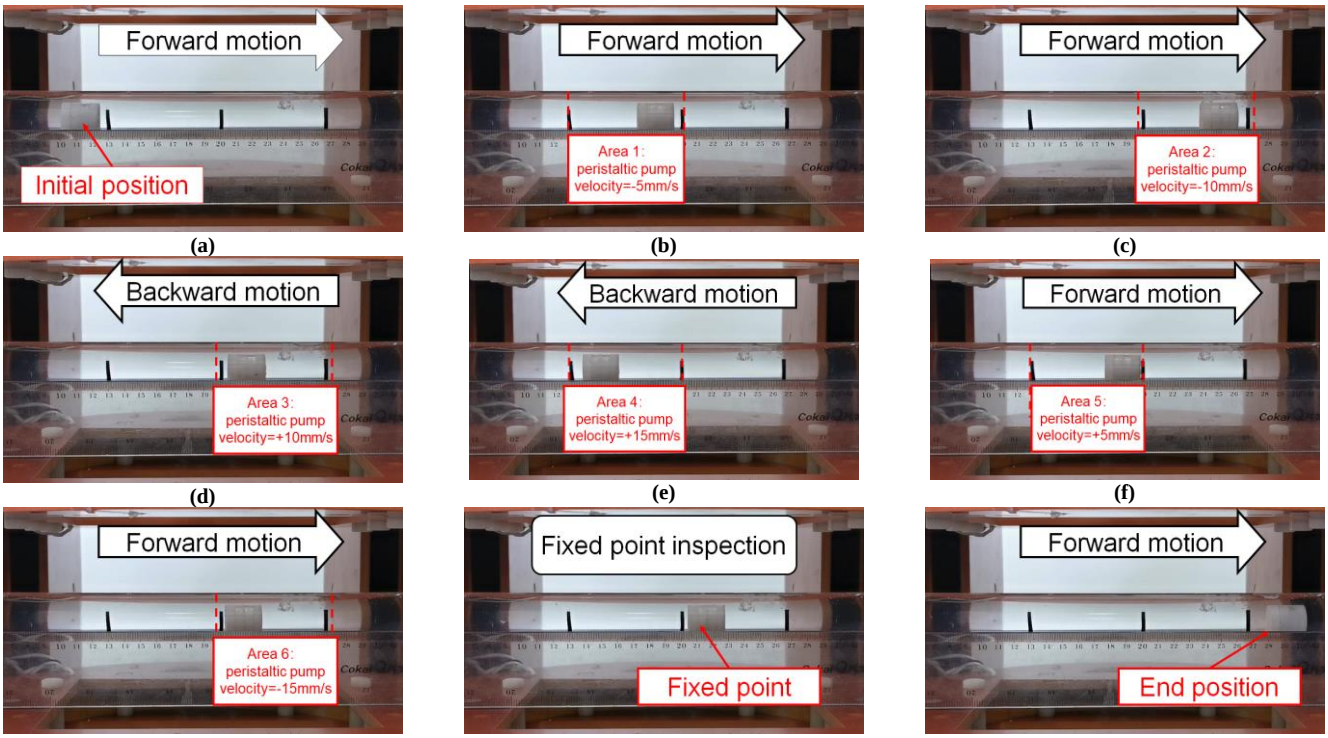

Fig. 18. The displacement of microrobot. (a) shows microrobot in initial position. (b-c) shows that the forward motion of microrobot in the area 1 with peristalsis velocity of -5 mm/s and the area 2 with peristalsis velocity of -10 mm/s respectively. (d-e) shows that the backward motion of microrobot in the area 3 with peristalsis velocity of +10 mm/s and the area 4 with peristalsis velocity of +15 mm/s respectively. (f-g) shows that the forward motion of microrobot in the area 5 with peristalsis velocity of +5 mm/s and the area 6 with peristalsis velocity of -15 mm/s respectively. (h) shows that the microrobot stops at the fixed point in the area 6 with peristaltic velocity of -15 mm/s for inspection task. (i) shows microrobot in end position.

accurately controlled, it only needs to be in the control area where the magnetic field frequency does not exceed the stability.

Multiple reciprocating motions are designed to simulate the clinical examination process of human intestinal peristalsis at different velocities. The relationship between the microrobot velocity and the peristaltic pump velocity and the displacement of the microrobot in the whole process is shown in Fig. 17. Firstly, the microrobot moved forward in area 1 with a peristalsis velocity of –5 mm/s; and moved forward in area 2 with a peristalsis speed of -10 mm/s. Then the microrobot moves back and forth in area 3 with a peristalsis speed of +10 mm/s. Then the microrobot moves back in area 4 with a peristalsis speed of +15 mm/s. Then the microrobot moves forward in area 5 with a peristalsis speed of + 5 mm/s. When the peristalsis speed of -15 mm/s area 6 is reached, the robot cannot stay in the intestinal tract due to the peristalsis of the intestinal tract, and it needs to maintain a similar speed to achieve the purpose of accurate inspection in the diagnosis area. Therefore, by controlling the microrobot's frequency characteristics, its speed is about -15 mm/s, so it can stay in area 6 and hardly move. After the inspection, the microrobot moved forward and was discharged from the pipe. The experimental results are shown in Fig. 18.

VI. Conclusions

This paper focuses on the structure and control method optimization of the magnetically driven spiral jet microrobot. The microrobot comprises a spiral structure and a protective shell, with space for embedding the functional module. Based on the dynamic model of the microrobot, the influence of the structure parameters of the microrobot on the motion performance is analyzed by using FDM. The fluid simulation of the microrobot is carried out using the finite element method, and the influence of the propulsion and resistance of the microrobot on the motion is obtained. By changing the frequency of the rotating magnetic field to adjust the speed of the microrobot, it has been verified that the microrobot still has good flexibility in the static fluid and peristaltic pump simulation intestinal system. Whether it is a platform that uses a permanent magnet and motor consolidation to control the movement of the microrobot in a single direction [34] or a control platform that uses a micro coil to power the microrobot [35] wirelessly, the MACMS in this paper can realize the movement in any direction, which is suitable for clinical application.

Meanwhile, compared with the microrobot with bare threaded shell [36], the microrobot in this paper can nload modules and protect the intestinal tract. In addition, by optimizing the structure design and control method of the microrobot in this paper, the microrobot can maintain better flexibility in the environment with the change of peristaltic speed, which significantly improves the adaptability of the microrobot to the human intestinal peristaltic environment. In the future, we will focus on developing multiple functions in the magnetic drive microrobot, and design some experiments to simulate the realization of medical functions.

REFERENCES

[1] Z. Liao, G. Wang, G. Chen, W. Zou, and X. Jiang, “Clinical practice consensus for magnetically controlled capsule gastroscopy,” *Chin J Pract Intern Med*, vol. 37, no. 10, pp. 885-894, 2021.

[2] L. Zheng, S. Guo, Z. Wang and T. Tamiya, "A multi-functional module-based capsule robot," *IEEE Sens. J.*, vol. 21, no. 10, pp. 12057-12067, 2021.

[3] M. Yu, “M2A™capsule endoscopy: A breakthrough diagnostic tool for small intestine imaging,” *Gastroenterol Nurs*, vol.25, pp. 24–27, 2002.

[4] G. Iddan, G. Meron, A. Glukhovsky, P. Swain, “Wireless capsule endoscopy,” *Nature*, vol.405, pp. 417-418, 2000.

[5] M. Simi, P. Valdastri, C. Quaglia, A. Menciassi and P. Dario, "Design, fabrication, and testing of a capsule with hybrid locomotion for gastrointestinal tract exploration," *IEEE ASME Trans Mechatron*, vol. 15, no. 2, pp. 170-180, 2010.

[6] M. Sitti, "Miniature soft robots — road to the clinic." *Nat. Rev.*, vol. 3, pp. 74-75, 2018.

[7] J. Abbott, K. Peyer, M. Lagimarsino, L. Zhang, L. Dong, I. Kaliakatsos, B. Nelson, “How should microrobots swim?” *Int J Rob Res*, vol. 28, no. 11–12, pp. 1434–1447, 2009.

[8] J. Rahmer, C. Stehning, and B. Gleich, “Spatially selective remote magnetic actuation of identical helical micromachines,” *Sci. Robot.*, vol. 2, no. 3, pp. eaal2845, 2017.

[9] X. Jin, S. Guo, J. Guo, P. Shi, T. Tamiya, and H. Hirata, "Development of a tactile sensing robot-assisted system for vascular interventional surgery," *IEEE Sens. J.*, vol. 21, no. 10, pp. 12284-12294, 2021.

[10] M. Geng, A. Wang, W. Gao, Z. Zhang, Y. Xiong, and Y. Li, “Diagnostic value of OMOM capsule endoscopy in gastrointestinal diseases,” *J. Clin. Gastroenterol.*, vol. 22, no. 1, pp. 13-16, 2010.

[11] K. Peyer, L. Zhang, B. Nelson, “Bio-inspired magnetic swimming microrobots for biomedical applications,” *Nanoscale*, vol. 5, no. 4, pp. 1259–1272, 2013.

[12] F. Munoz, G. Alici, H. Zhou, W. Li, and M. Sitti, “Analysis of magnetic interaction in remotely controlled magnetic devices and its application to capsule robot for drug delivery,” *IEEE/ASME Trans. Mechatronics*, vol. 3, no. 1, pp. 298-310, 2018.

[13] Q. Fu, S. Guo, Q. Huang, H. Hirata, and H. Ishihara, “Development and evaluation of novel magnetic actuated microrobot with spiral motion using electromagnetic actuation system,” *J. Med. Biol. Eng.*, vol. 36, no. 4, pp. 506–514, 2016.

[14] Y. Zhang, D. Yang, D. Wang, “Polarization criteria detection of a generalized spatial universal rotating magnetic vector,” *IEEE Trans. Magn.* Vol. 54, no. 7, pp. 1-8, 2018.

[15] Y. Zhang, S. Jiang, X. Zhang, X. Ruan, D. Guo, “A variable-diameter capsule robot based on multiple wedge effects,” *IEEE/ASME Trans Mechatron*, vol. 16, no. 2, pp. 241-254, 2011.

[16] S. Yim, M. Sitti, “Design and rolling locomotion of a magnetically actuated soft capsule endoscope,” *IEEE Trans. Robot*, vol. 28, no. 1, pp. 183-194, 2012.

[17] S. Kim, J. Lee, S. Hashi, K. Ishiyama, “Oscillatory motion-based miniature magnetic walking robot actuated by a rotating magnetic field,” *Rob Auton Syst*, vol. 60 no. 2, pp. 288-295, 2012.

[18] Q. Fu, S. Guo, Y. Yamauchi, H. Hirata, and H. Ishihara, “A novel hybrid microrobot using rotational magnetic field for medical applications,” *Biomed. Microdevices*, vol. 17, no. 2, pp. 31-42, 2015.

[19] Q. Fu, S. Zhang, S. Guo, and J. Guo, “Performance evaluation of a magnetically actuated capsule microrobotic system for medical applications,” *Micromachines*, vol. 9, no. 12, pp. 641-656, 2018.

[20] H. Zhou, G. Alici, T. Than, W. Li, “Modeling and experimental characterization of propulsion of a spiral-type microrobot for medical use in gastrointestinal tract,” *IEEE. Trans. Biomed. Eng*, vol. 60 no. 6, pp. 1751-1759, 2013.

[21] D. Pham, S. Aziz, “A real-time localization system for an endoscopic capsule using magnetic sensors,” *Sensors*, vol. 14, pp. 20910-20929, 2014.

[22] Q. Fu, S. Guo, S. Zhang, “Characteristic evaluation of a shrouded propeller mechanism for a magnetic actuated microrobot,” *Micromachines*, vol. 6, no. 9, pp. 1272–1288, 2015.

[23] L. Zhang, J. Abbott, L. Dong, K. Peyer, B. Kratochvil, H. Zhang, C. Bergeles, B. Nelson, “Characterizing the swimming properties of artificial bacterial flagella,” *Nano Lett*, vol. 9, no. 10, pp. 3663–3667, 2009.

[24] Q. Shi, T. Liu, S. Song, J. Wang, and M. Q.-H. Meng, "An optically aided magnetic tracking approach for magnetically actuated capsule robot," *IEEE Trans Instrum Meas*, vol. 70, pp. 1-9, 2021.

[25] M. Wang, S. Song, J. Liu, and M. Q.-H. Meng, "Multipoint simultaneous tracking of wireless capsule endoscope using magnetic sensor array," *IEEE Trans Instrum Meas*, vol. 70, pp. 1-10, 2021.

[26] Q. Fu, Z. Cai, J. Guo, S. Guo, “Evaluation performance of the magnetic rotational field for magnetically actuated microrobot system,” In Proceedings of 2020 IEEE international conference on mechatronics and automation, pp. 1396-1400, 2020.

[27] Y. Zhang, H. Yu, X. Ruan, N. Wang, D. Guo, “Kinematics characteristics of a new capsule-type micro microrobot in intestine,” *J. Mech. Eng*, vol. 45, pp. 18-23, 2009.

[28] Z. Bao, “Study on structure and control of targeted drug delivery multi-modular capsule robot system,” M.S. thesis, TJUT. Univ, TNJ, CHN, 2020.

[29] ANSYS®, Academic research, release 18.1, ANSYS FLUENT, *Theory Guide, ANSYS, Inc*, 2020.

[30] S. Guo, Y. He, L. Shi, S. Pan, R. Xiao, K. Tang, G. Ping, “Modeling and experimental evaluation of an improved amphibious robot with compact structure,” *Robot Comput Integr Manuf*, vol. 51, pp. 37-52, 2018.

[31] X. Hou, S. Guo, L. Shi, H. Xing, Y. Liu, H. Liu, Y. Hu, D. Xia, Z. Li “Hydrodynamic analysis-based modeling and experimental verification of a new water-jet thruster for an amphibious spherical robot,” *Sensors*, vol. 19, no. 2, 2019.

[32] J. Guo, Z. Bao, Q. Fu, S. Guo, “Design and implementation of a novel wireless modular capsule robotic system in pipe,” *Med Biol Eng Comput*, vol. 58, pp. 6785, 2020.

[33] P. Zhang, “Study on the structure and control of magnetic multi-modular capsule robotic system,” M.S. thesis, TJUT. Univ, TNJ, CHN, 2019.

[34] B. Ye, Z. Zhong, W. Zhang and D. Hu, "Research on coaxial control of magnetic spiral-Type capsule endoscope," *IEEE Access*, vol. 8, pp. 108113-108120, 2020.

[35] L. Liang, B. Chen, Y. Tang, Y. Xu, Y. Liu, “Operational performance analysis of spiral capsule robot in multiphase fluid,” *Robotica*, vol. 37, no. 2, pp. 213-232, 2019.

[36] S. Guo, Q. Yang, L. Bai, Y. Zhao, “Development of multiple capsule robots in Pipe,” *Micromachines*, vol. 9, no. 6, 2018.

Zhuocong Cai is currently working toward the M.S degree in College of Electrical and Electronic Engineering from Tianjin University of Technology, Tianjin, China. His research interests include the design of the magnetic actuated microrobot, the electromagnetic drive system, and design of the self-reconfigurable microrobot.

Qiang Fu received the Ph.D. degree in intelligent mechanical systems engineering from Kagawa University, Takamatsu, Japan, in 2017. He is currently an associate professor in Tianjin University of Technology, Tianjin, China. His current research is on biomedical robots, such as the development of multi-module magnetic actuated microrobotic systems for biomedical applications.

Songyuan Zhang received the Ph.D. degree in intelligent mechanical systems engineering from Kagawa University, Takamatsu, Japan, in 2016. He is currently an associate professor in State Key Laboratory of Robotics and System, Harbin Institute of Technology, China. His research interests include bio-inspired robotics, human robot interaction and medical robots.

Shuxiang Guo (SM'03, F'21) received the Ph.D. degree in Mechanoinformatics and Systems from Nagoya University, Japan, in 1995. He is currently a full professor at the Faculty of Engineering and Design, Kagawa University, Japan. He received the Chang Jiang Professor-ship Award from the Ministry of Education of China, in 2005. Dr. Guo is Editor in chief for the *International Journal of Mechatronics and Automation*.

Jian Guo received the Ph.D. degrees in intelligent machine system from Kagawa University, Japan, in 2012. He is currently a full professor in Tianjin University of Technology, Tianjin, China. His current research is on biomedical robots, such as wireless microrobots in pipe and robotic catheter systems for biomedical applications.

Xi Zhang is currently working toward the M.S degree in College of Electrical and Electronic Engineering from Tianjin University of Technology, Tianjin, China. Her research interests include the design and control method of the microrobot.

Chunliu Fan is currently working toward the M.S degree in College of Electrical and Electronic Engineering from Tianjin University of Technology, Tianjin, China. Her research interests include the design and control method of the microrobot.